Journal of Power Sources 195 (2010) 7432–7437

Contents lists available at ScienceDirect

Journal of Power Sources

journal homepage: www.elsevier.com/locate/jpowsour

Fabrication and lithium storage performance of three-dimensional porous NiO as anode for lithium-ion battery

Chong Wang, Dianlong Wang*, Qiuming Wang, Huanjun Chen

School of Chemical Engineering & Technology, Harbin Institute of Technology, Harbin 150001, China

ARTICLE INFO

Article history:
Received 12 January 2010
Received in revised form 21 April 2010
Accepted 22 April 2010
Available online 27 May 2010

Keywords:
Three-dimensional
Porous
Nickel oxide
Thermal treatment
Lithium-ion batteries

ABSTRACT

Three-dimensional porous NiO is prepared on Ni foam by a thermal treatment method at various temperatures. The morphology and structure of porous NiO are characterized by X-ray diffraction, scanning electron microscopy and transmission electron microscopy. The electrochemical properties of three-dimensional porous NiO anode are evaluated by galvanostatic discharge–charge cycling, cyclic voltammery, and impedance spectral measurements on cells with lithium as the counter and reference electrodes. Results show that porous NiO delivers a stable capacity of $520 \pm 20\,mAh\,g^{-1}$ with no noticeable capacity fading up to 30 cycles when cycled in the voltage range 0.05–3.0 V at rate of 0.2 C. The porous NiO exhibits higher reversible capacity, better cycleability, as well as higher rate capability in comparison to NiO foil. The observed cyclic voltammograms and impedance spectra are analyzed and interpret a redox reaction of NiO–Ni^0 with formation and decomposition of Li_2O. The excellent electrochemical performance of porous NiO can be attributed to its large surface area, which lowers the current density of NiO reaction interface, and then an alternative anode is provided for lithium-ion batteries.

1. Introduction

The increasing demand for higher capacity batteries in electronics devices has promoted an intense research effort to develop new materials with high gravimetric and volumetric charge capacity and excellent cycleability suitable for high-energy capacity lithium (Li) batteries. Due to their high theoretical energy densities, a number of transition metal oxide MO (such as CoO, CuO, NiO, etc.) electrode materials, based on a novel conversion mechanism, have also been investigated as candidates for negative electrodes in the past few years [1–3]. However, most of the transition metal oxides usually suffer from the problems of poor electronic conduction and poor capacity retention performance using as anode materials.

Using of nanostructured electrode materials could partly solve these problems for the high specific surface which increase the contact of active material with carbon additives, short Li diffusion path and excellent accommodation of the strains of Li insertion/extraction [1,4–6], whereas, the high surface area increased the decomposition of electrolyte on active materials which causes a high level of irreversible capacity and poor cycleability [7]. Recently, three-dimensional structure electrodes have attracted great interest in both fundamental as well as applied research areas due to their large surface area and short ion diffusion distance compared to two-dimensional plate electrodes [8,9]. Construction of well-ordered, various models of 3D structures electrodes and realization of their potential applications have resulted in intensive research for the past few years. In these, fabricating three-dimensional porous electrodes has provided a simple but efficient approach to improve the reversible capacity and rate capability of MO anodes [10,11]. For example, Yu et al. [12] demonstrated that Ni foam supported CoO–Li_2O exhibited excellent electrochemical performance in lithium-ion batteries. Furthermore, Gillot et al. reported that the growth of carbon-free, self-supported nickel diphosphide onto Ni foam, which showed enhanced capacity retention and rate capabilities [13].

In this paper, we reported a thermal treatment method to successfully synthesize three-dimensional porous NiO electrodes on Ni foam substrate as a superior anode material for lithium-ion batteries. It is found that porous NiO electrode exhibited not only excellent cycling stability and high reversible capacity, but also high-rate performance in comparison to foil structure electrodes. As a result, the as-prepared porous NiO exhibited high specific capacity ($520(\pm 20)\,mAh\,g^{-1}$ at 0.2 C), significantly improved cycling performance, and high-rate performance compared to NiO foil, suggesting its potential use as anode electrode for Li-ion batteries.

2. Experimental

2.1. Preparation of three-dimensional porous NiO

Ni foam with NiO film was synthesized by thermal treatment method. Ni foam (100PPI pore size, $500\,g\,m^{-2}$ surface density, Inco

* Corresponding author. Tel.: +86 0451 86413751; fax: +86 0451 86221048.
E-mail address: chinawangchong@126.com (D. Wang).

0378-7753/$ – see front matter © 2010 Elsevier B.V. All rights reserved.
doi:10.1016/j.jpowsour.2010.04.090

Co., China) with thickness of 300 μm was used both as supporting substrate as well as source of metal precursor for the growth of NiO film. In typical procedure, prior to thermal treatment, Ni foam was washed with ethyl alcohol and deionized (DI) water for several times, and dried in a cool air stream. The pretreated Ni foams were then put into the center of heating quartz tube. The growth of NiO film was then initiated by step increase oxidation temperature (10 °C min^{-1}) in air. After growth, the samples were cooled down naturally to room temperature. Growth of film was carried out over a temperature range of 500–700 °C. Different surface morphologies were found at different thermal treatment temperatures of 500–700 °C. After growth, the shiny metallic surface of the nickel foam turned greenish yellow, indicating the presence of NiO film. The surface area per apparent unit area of porous NiO was approximately 120 m^2 m^{-2} measured by the BET method.

2.2. Measurement of structural and electrochemical properties

The morphology and microstructure of the as-synthesized three-dimensional porous NiO electrodes were characterized using field emission scanning electron microscopy (FESEM, Hitachi, S-4700) and transmission electron microscopy (Hitachi, S-4700-7650), X-ray diffraction (XRD) was performed on Rigaku D/MAX-RC X-ray diffractometer with Cu Kα1 (45 kV, 50 mA, step size = 0.02°, 10° < 2θ < 100°) monochromated radiation in order to identify the crystalline phase of the materials. For electrochemical measurements, three-dimensional porous NiO was used as working electrode, Li metal foil (200 μm thick; China) was used as the counter (anode) and reference electrodes, and 1 M $LiPF_6$ (battery grade) dissolved in a mixture of ethylene carbonate (EC, battery grade) and dimethyl carbonate (DMC, battery grade) (1:1 by volume) was used as the electrolyte. And a Celgard 2300 (polypropylene) was used as the separator. Coin-type test cells (size 2025) were fabricated in an argon-filled glove box (Nanjin, China). The mass of active NiO was determined by the method described in Ref. [14]. The active mass of the material was calculated to be about 2–10.0 mg by the method described in Ref. [14]. The cells were aged overnight before measurement. Charge–discharge performance of the cell was characterized galvanostatically on BTS 5 V/10 mA battery testing system (Neware, Shenzhen, China) at about C/5 charge–discharge rate between 0.05 and 3.0 V (*vs.* Li/Li^+), and cyclic voltammetry (CV) was measured on an electrochemical workstation (CHI 630B) at a scan rate of 0.05 mV s^{-1} between 0.05 and 3.0 V (*vs.* Li/Li^+), respectively. Electrochemical impedance measurements were carried out with an electrochemical workstation (CHI 660B). The frequency range was from 100 kHz to 0.01 Hz with an ac signal amplitude of 5 mV.

3. Results and discussion

3.1. Characterization of porous NiO

Fig. 1 shows the XRD patterns of as-prepared porous NiO at different thermal treatment temperatures. The diffraction peaks of the surface film thermal treated above 500 °C represent the typical character of a face-centered cubic (fcc) NiO phase [JCPDS 47-1049, space group: *Fm*3*m* (2 2 5)]. No impurity peaks are observed in the XRD patterns excluding Ni substrate diffraction peaks. Well crystallized structure was obtained when thermal treated at 500–700 °C, and with the temperature increasing, the intensities of the diffraction peaks become intense and sharp, indicating the higher crystallinity. The crystallite sizes of the porous NiO are estimated with the Scherrer equation, $D = 0.94\lambda/(B\cos\theta)$, indicate that the average crystallite sizes of the porous NiO are approximately 28.7, 40.1 and 50 nm for thermal treatment at 500, 600 and 700 °C,

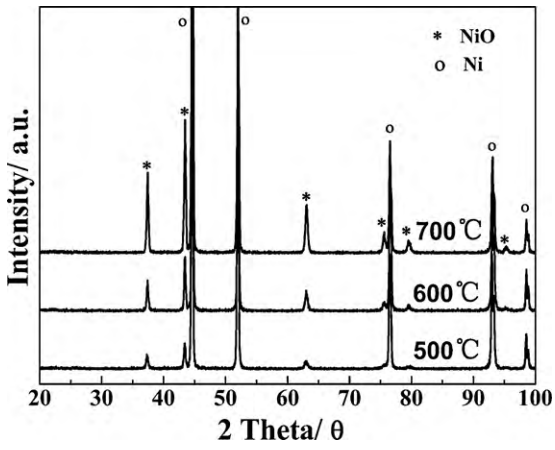

Fig. 1. XRD patterns of three-dimensional porous NiO thermal treated at various temperatures.

respectively (*D*: average dimension of crystallites, λ: wavelength of X-ray, *B*: full width at half maximum of a reflection located at 2θ) indicating the crystal size increases with the increase in the annealing temperature.

Fig. 2 shows the low- and high-magnification SEM images of porous NiO electrodes prepared at different thermal treatment temperatures (Fig. 2(a and d) 500 °C, (b and e) 600 °C, (c and f) 700 °C). As-prepared porous NiO electrodes from 500 °C thermal treatment show a uniform and crackless surface oxide film. The TEM image as shown in the insert image in Fig. 2d exhibits the film consisted nanoparticle subunits, which are approximately 100 nm in dimension. For the porous NiO from 600 °C thermal treatment, the film morphology is significantly different. From the magnified image, a dense and uniform oxide film is found. The film was micrometer scale in thickness (cross-side images are not shown in this paper). A rough film can be observed from the magnified images of porous NiO electrodes prepared at 700 °C. The film is nanopores structure consists of NiO nanowalls with thickness of several hundred nanometers. Different morphology can be formed at various thermal treatment temperatures. Poizot et al. suggest that for each metal oxide system there is an optimum precursor particle size and hence the best electrochemical performance [1]. So the difference morphology and surface particle size of porous NiO prepared at various thermal treatment temperatures will strongly affect the electrochemical performance.

3.2. Electrochemical studies

3.2.1. Galvanostatic cycling

The electrochemical performance of as-prepared porous NiO electrodes for Li-ion batteries was evaluated by galvanostatic discharge/charge cycling and cyclic voltammetry. The voltage *vs.* capacity curves of as-prepared porous NiO electrodes prepared at 600 °C are shown in Fig. 3a. The first discharge/charge cycle curves for different thermal treatment temperatures are shown in Fig. 3b. As shown in Fig. 3a and b, the voltage decreased rapidly to about 0.6 V during the first discharge, and a plateau region maintained until a capacity of 794 mAh g^{-1} was reached which corresponds to a consumption of 2.0 mol of Li per mol of NiO. The first charge profile of porous NiO shows voltage plateaus at 2.2 V. The second and following discharge curves differed from the first, suggesting drastic, lithium driven, structural or textural modifications [1]. The capacity *vs.* cycle number curves at different thermal treatment temperatures are shown in Fig. 3c. The first discharge–charge capacities were 772 and 588 mAh g^{-1}, 794 and 567 mAh g^{-1}, 886 and 588 mAh g^{-1} for thermal treat-

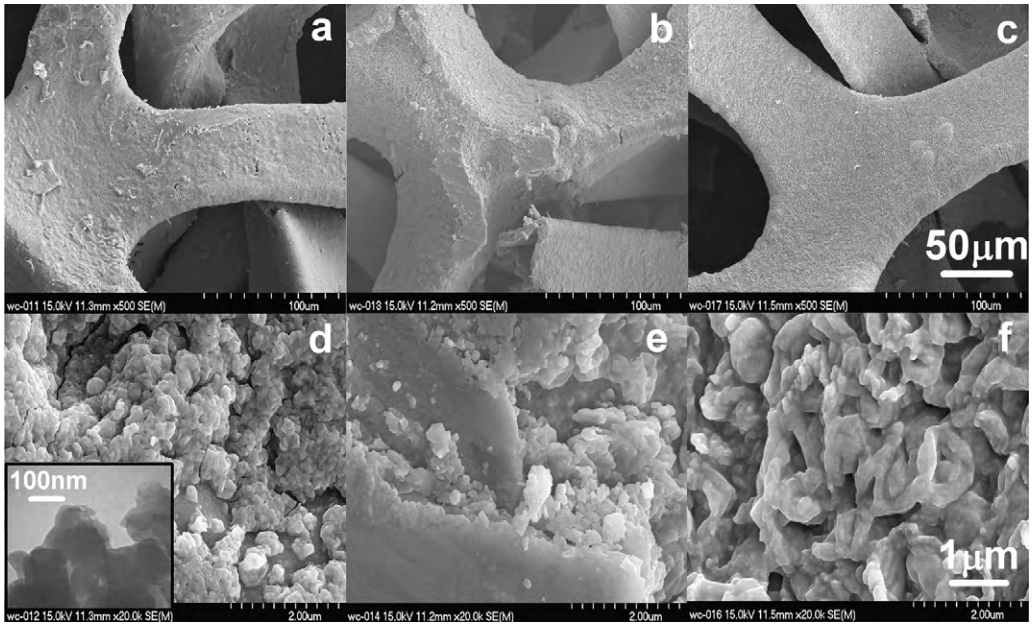

Fig. 2. SEM images of three-dimensional porous NiO thermal treated at different temperatures: (a and d) 500 °C, (b and e) 600 °C, and (c and f) 700 °C (insert image in (d) is the TEM images of porous NiO prepared at 500 °C).

ment at 500, 600 and 700 °C, respectively. The irreversible capacity losses were 184, 227 and 298 mAh g^{-1}, respectively. The results showed that charge/discharge performance and cycleability of porous NiO prepared at 500 °C were better than 600 and 700 °C, which indicates that low thermal-treatment temperature and small crystallite size could contribute to the enhanced electrochemical performance. Irreversible capacity loss during first cycle is most caused by formation of solid electrolyte interface (SEI) and incomplete decomposition of Li_2O at the first discharge [15,16]. A previous report on the electrochemical performance of 2D structure NiO electrode showed a discharge capacity around 750 and 300 mAh g^{-1} at the end of the 2nd and 30th cycles respectively, cycled between 0.01 and 3.0 V, at a rate of 0.1 C [17]. In the present study, porous NiO exhibiting less than 7% capacity fade between

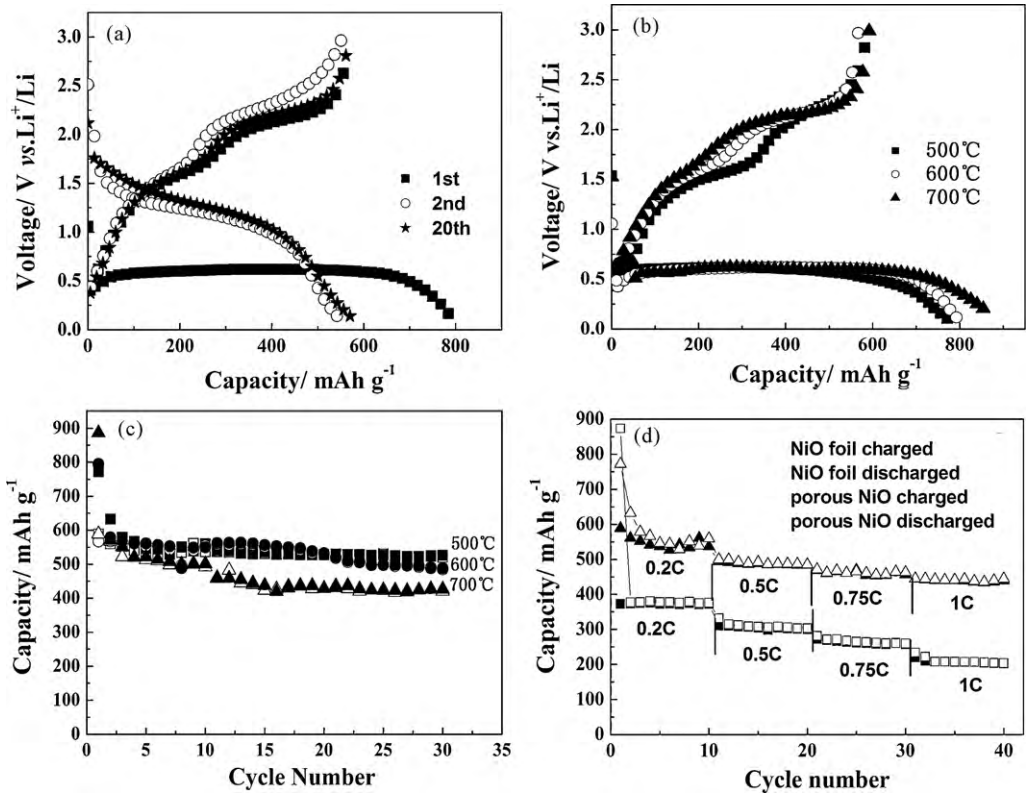

Fig. 3. (a) Charge/discharge curves of three-dimensional porous NiO (600 °C thermal treatment), (b) the first charge/discharge curves of three-dimensional porous NiO, (c) cycleability of three-dimensional porous NiO, cycled between 3.0 and 0.05 V *vs.* Li/Li^+, at current density 0.2 C and (d) rate performance of cells with NiO foil and porous NiO anodes.

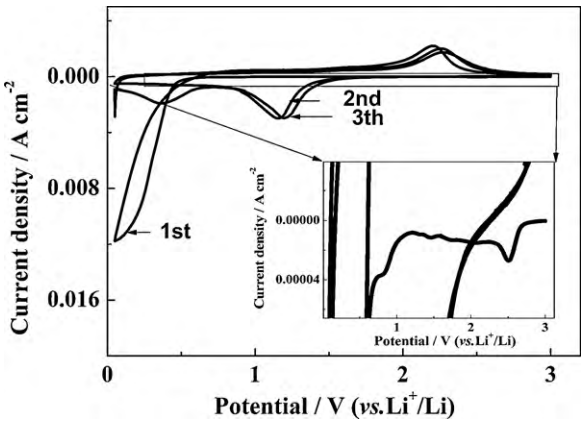

Fig. 4. CV curves of three-dimensional porous NiO; scan rate 0.05 mV s^{-1}.

2 and 30 cycles at a current density 0.2 C rate. Fig. 3d is rate performance of cells with different anodes charged/discharged at various rates. It can be seen that capacity decreased as discharge-charge rate increased. However, the capacity of cells with NiO foils anode dropped more rapidly than that of porous NiO anode. At rate of 1 C, only 54% discharge capacity of 0.2 C rate was obtained for cell with NiO foil anode, while cell with porous NiO anode was able to retain 82% discharge capacity, suggesting that porous NiO anode favors high-rate charge/discharge application. The as-prepared porous NiO shows a larger surface area compared to its NiO foil counterpart, which makes the enhanced electrochemical performance of porous NiO. A previous reports on the electrochemical performance of NiO film electrode showed a discharge capacity around 330 mAh g^{-1} at the end of 30th cycles at a rate of 0.11 C [18]. In the present study, 3D porous Co_3O_4 did not exhibited obvious capacities fade up to 50 cycles with a high current density of 718 mA g^{-1} (1 C), which could be attributed to its unique 3D porous structure which can offer a larger materials/electrolyte contact area and accommodate the strain induced by the volume change during charge/discharge. It should be noted that though a three-dimensional porous structure may improve the electrochemical performance of electrodes, it may also decrease the specific volume capacity of lithium batteries. However, the reversible capacity of porous NiO is approximately 2 times that of commercial graphite electrodes. This high capacity compensates the decreased volume capacity caused by the porous structure substrate itself. Furthermore, the thickness of NiO films on nickel foam can be increased with longer process time. Therefore, the volume capacity decrease due to the porous structure will be limited compared to commercial graphite electrodes [18].

3.2.2. Cyclic voltammetry (CV)

The CV curves of the porous NiO were tested at a scan rate of 0.05 mV s^{-1} in the voltage range 0.05–3.0 V, as shown in Fig. 4. A small continuous reactive current and a small reactive peak can be found in the first catholic scan started from open circuit voltage (OCV 3.0 V) (inset figure in Fig. 4) indicating the formation of surface film (SEI) has already started above 2.0 V during the first cathodic scan. A large cathodic current peak started at 0.6 V corresponding to the initial reduction of $Ni^{2+}O$ to metallic Ni, accompanying the formation of Li_2O. In the first anodic scan, one anodic peak at 2.2 V is found, which corresponding to the NiO formation, accompanying the decomposition of Li_2O [19,20], which all well correspond to the discharge/charge plateaus displayed in Fig. 3b. Compared with the first cycle, a set of broad peaks at 1.2 and 2.2 V were observed, respectively. It worth noted that a small peak started at about 0.5 V on the second cycle appeared which corresponded to incomplete activation of electrode materials at first cycle. After the electrode activation during first cycle, the well-overlapped of the second and third cycles curves indicated the stable electrochemical process has been set up. The CV curves of the porous NiO are qualitatively similar to the results obtained by Varghese et al. [19], and the reaction mechanism is shown as follows [1,19]:

$$NiO + 2Li^+ + 2e^- \rightarrow Ni^0 + Li_2O + \frac{\text{polymeric layer formation}}{\text{electrolyte reduction}} \quad (1)$$

$$Ni^0 + Li_2O \rightarrow NiO + 2Li^+ + 2e^- \quad (2)$$

3.2.3. Electrochemical impedance spectroscopy

Impedance measurements were carried out at room temperature on cells with porous NiO at selected discharge capacity in the range of 0.05–3.0 V at a charge/discharge current density of 356 mA g^{-1} during the first discharge/charge cycle. The cells were discharged or charged to a particular discharge capacity value (mAh g^{-1}) and relaxed for 1 h and the impedance was measured. The Nyquist plots at various discharge capacity values during the first discharge cycle are shown Fig. 5a. The inset figure is the zoom part at the range of high frequency. The impedance spectra of the cells are composed of two merged semicircles and a straight sloping line which corresponding to the resistance of the surface film, charge-transfer resistance and the Warburg impedance. The impedance data were analyzed by fitting to an equivalent electrical circuit similar to other reports [21], which is made up of a serial connection of R_e, $R_{sf}//C_{sf}$, $R_{ct}//C_{dl}$, Z_w and C_{ini} as shown in Fig. 5c. It consists of electrolyte (R_e), surface film (R_{sf}) and charge-transfer resistance (R_{ct}), Warburg impedance (Z_w) and intercalation capacitance (C_{ini}), respectively.

The fresh cell (at OCV) shows a single broad depressed semicircle in the high-frequency region (>1 kHz). It indicates that the porous NiO at OCV state has larger polarization resistance which attributed mainly to larger surface film resistance (R_f) and the curve fitting was carried out using $R_{(sf+ct)}$ combination. Spectrum measured at the discharge depth of 179.5 mAh g^{-1} differs markedly from the initial one. The semicircle decreases drastically with the deepening of discharge, and then drops to a relative steady value which indicates the formation of stable surface film. At the same time, a new semicircle appeared with the deepening of discharge which is related to the charge-transfer resistance at interface (R_{ct}) and R_{ct} comes into prominence because of the initiation of the intercalation/decomposition reaction of lithium into porous NiO. Due to the observed two semicircles, the experimental data are simulated by an electrical equivalent circuit composed of two $C//R$ ($C_{sf}//R_{sf}$ and $C_{dl}//R_{ct}$) elements in series. The R_{ct} should not increase since more active reaction sites and conductive Ni atoms are produced with the deepening of discharge. The spectra measured in the discharge depth range 179.5–538.5 mAh g^{-1} are qualitatively similar. On the other hand, the spectrum recorded at 0.05 V, the deep discharge limit, shows a large-diameter semicircle. The impedance spectra during the first charge cycle are qualitatively similar and are shown in Fig. 5b.

The XRD patterns of cycled electrodes in their charged and discharged state are shown in Fig. 6a, and SEM images of the electrode in the charged and discharge state (after 30 cycles) are shown in Fig. 6b and c. The results show that only the diffraction peaks of the nickel substrate can be identified, no NiO diffraction peaks were found after discharge/charge cycling. The initial NiO film structure (shown in Fig. 2) has been modified during cycling and some texture structures on initial film disappeared. The XRD patterns and SEM images of cycled electrodes in their charged or discharged state suggest that initial NiO film (as shown in Fig. 2) has transformed to amorphous/nanosized particles during cycling. Similar structure and morphology variations are reported in literatures [1,19,22–24].

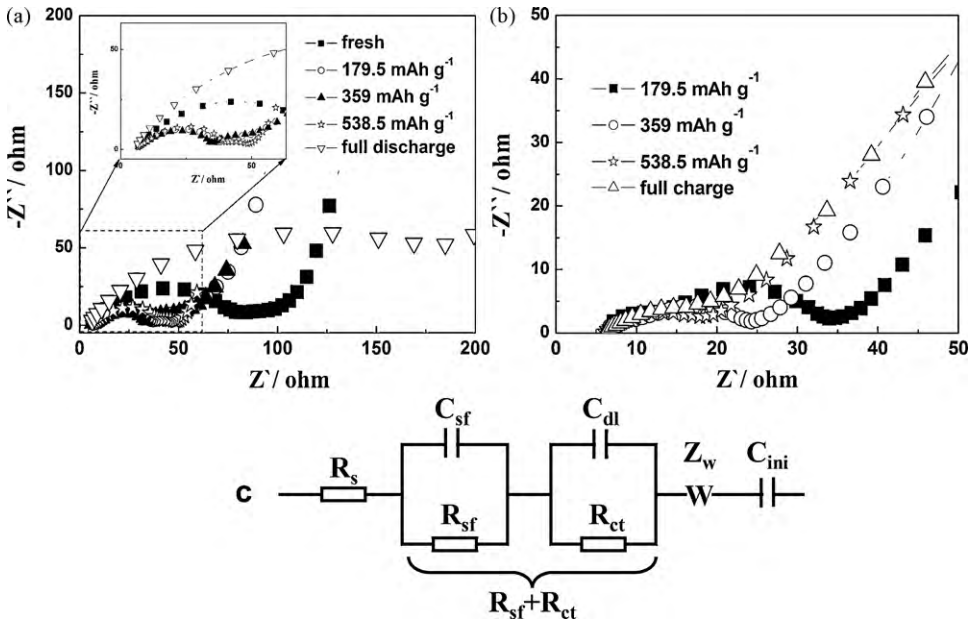

Fig. 5. (a) Nyquist plots of three-dimensional porous NiO during the first discharge, and (b) first charge, at various discharged state, the inset figure is the zoom part at high frequencies region; (c) equivalent electrical circuit.

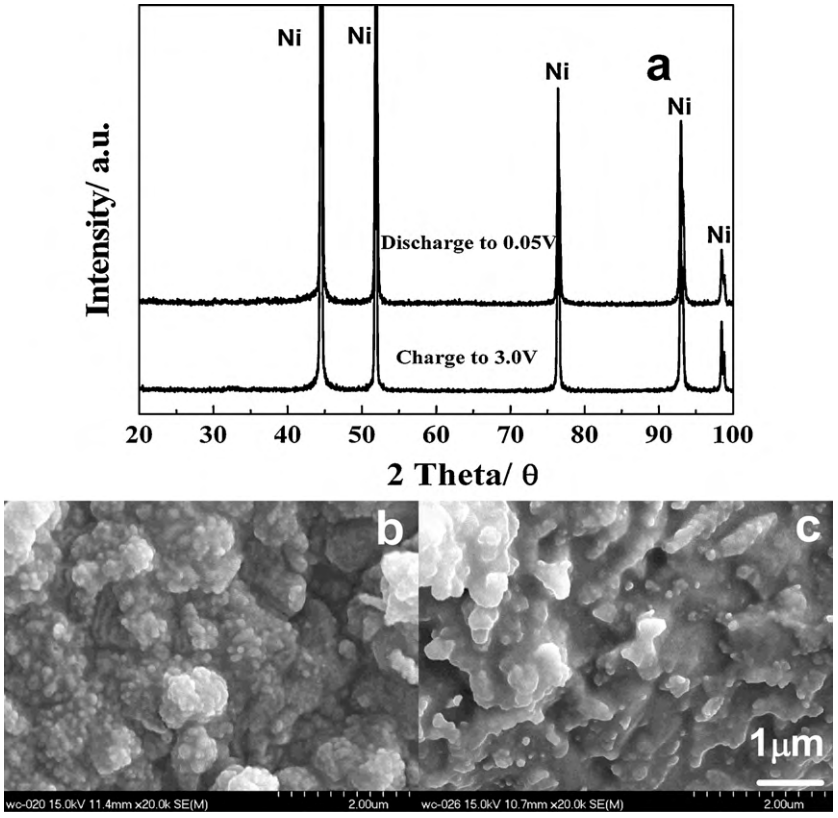

Fig. 6. (a) XRD patterns of three-dimensional porous NiO at full charged/discharged states. SEM images of three-dimensional porous NiO at full charged/discharged states, (b) discharged to 0.05 V and (c) charged to 3.0 V.

4. Conclusion

A simple thermal treatment method to prepare large surface area porous NiO directly on Ni foam was presented. The as-prepared porous NiO was characterized by SEM, TEM and XRD. Electrochemical properties of porous NiO showed high discharge/charge capacity, excellent capacity retention and rate performance in comparison to NiO foil, which makes porous NiO a promising anode material for high power Li-ion batteries. The high capability and cycleability of porous NiO electrodes are better

than the previously reported works on 2D structure NiO electrodes can be attributed to its large surface area, which lower the current density and polarization of NiO.

Acknowledgement

This work has been supported in part by National Natural Science Foundation of China (No. 50974045).

References

[1] P. Poizot, S. Laruelle, S. Grugeon, L. Dupont, J.M. Tarascon, Nature 407 (2000) 496–499.
[2] P. Poizot, S. Laruelle, S. Grugeon, J.M. Tarascon, J. Electrochem. Soc. 149 (2002) A1212–A1217.
[3] X. Wang, J.M. Song, L.S. Gao, J.Y. Jin, H.G. Zheng, Z.D. Zhang, Nanotechnology 16 (2005) 37–39.
[4] A.M. Cao, J.S. Hu, H.P. Liang, L.J. Wan, Angew. Chem. Int. Ed. 44 (2005) 4391–4395.
[5] S. Grugeon, S. Laruelle, R.H. Urbina, L. Dupont, P. Poizot, J.M. Tarascon, J. Electrochem. Soc. 148 (2001) A285–A292.
[6] F. Cheng, Z. Tao, J. Liang, J. Chen, Chem. Mater. 20 (2008) 667–672.
[7] O. Delmer, P. Balaya, L. Kienle, J. Maier, Adv. Mater. 20 (2008) 501.
[8] J.W. Long, B. Dunn, D.R. Rolison, H.S. White, Chem. Rev. 104 (2004) 4463–4492.
[9] D. Golodnitsky, V. Yufit, M. Nathan, I. Shechtman, T. Ripenbein, E. Strauss, S. Menkin, E. Peled, J. Power Sources 153 (2006) 281–287.
[10] X.H. Huang, J.P. Tu, X.H. Xia, X.L. Wang, J.Y. Xiang, Electrochem. Commun. 10 (2008) 1288–1290.
[11] P. Zhang, Z.P. Guo, S.G. Kang, Y.J. Choi, C.J. Kim, K.W. Kim, H.K. Liu, J. Power Sources 189 (2009) 566–570.
[12] Y. Yu, C.H. Chen, J.L. Shui, S. Xie, Angew. Chem. 117 (2005) 7247–7251.
[13] F. Gillot, S. Boyanov, L. Dupont, M.L. Doublet, M. Morcrette, L. Monconduit, J.M. Tarascon, Chem. Mater. 17 (2005) 6327–6337.
[14] H.B. Wang, Q.M. Pan, J.W. Zhao, G.P. Yin, P.J. Zuo, J. Power Sources 167 (2007) 206–211.
[15] X.H. Huang, J.P. Tu, B. Zhang, C.Q. Zhang, Y. Li, Y.F. Yuan, H.M. Wu, J. Power Sources 161 (2006) 541–544.
[16] A. Debart, L. Dupont, P. Poizot, J.B. Leriche, J.M. Tarascon, J. Electrochem. Soc. 148 (2001) A1266–A1274.
[17] X.H. Huang, J.P. Tu, C.Q. Zhang, J.Y. Xiang, Electrochem. Commun. 9 (2007) 1180–1184.
[18] H.B. Wang, Q.M. Pan, X.P. Wang, G.P. Yin, J.W. Zhao, J. Appl. Electrochem. 39 (2009) 1597–1602.
[19] B. Varghese, M.V. Reddy, Y.W. Zhu, Chem. Mater. 20 (2008) 3360–3367.
[20] S.A. Needham, G.X. Wang, H.K. Liu, J. Power Sources 159 (2006) 254–257.
[21] M.V. Reddy, T. Yu, C.H. Sow, Z.X. Shen, C.T. Lim, G.V. Subba Rao, B.V.R. Chowdari, Adv. Funct. Mater. 17 (2007) 2792–2799.
[22] M.V. Reddy, S. Madhavi, G.V. Subba Rao, B.V.R. Chowdari, J. Power Sources 162 (2006) 1312–1321.
[23] Y. Sharma, N. Sharma, G.V. Subba Rao, B.V.R. Chowdari, Adv. Funct. Mater. 17 (2007) 2855–2861.
[24] G.X. Wang, Y. Chen, K. Konstantinov, M. Lindsay, H.K. Liu, S.X. Dou, J. Power Sources 109 (2002) 142–147.